Journal of Marine Science and Application (2026) 25: 377-392
https://doi.org/10.1007/s11804-025-00781-7

RESEARCH ARTICLE

Comparative Analysis of the Impact of Geometrical Parameters on the Hydrodynamic Performance and Flow Characteristics of a Toroidal Propeller

Alireza Nadery[1], Hossein Shafigh[2], Amin Najafi[2], Hassan Ghassemi[1,3] and S. Yasin Ziabari[1]

Received: 14 December 2024 / Accepted: 25 May 2025

Abstract

This study parametrically explores the hydrodynamic characteristics of a toroidal propeller. Seven geometrical parameters (skew angle, pitch angle, chord length, rake, roll angle, blade alpha vertical angle, and blade section) are introduced, and their effects on thrust, torque, and efficiency are analyzed. The performance of the propellers is simulated using computational fluid dynamics based on the finite volume method. First, an open-water simulation is conducted for a common B-series propeller. The numerical results are compared with available experimental data, and an acceptable agreement is achieved. Then, the investigations were extended to the toroidal propeller by changing the seven geometrical parameters (±5%, ±10%, and ±20%). The analysis demonstrates hydrodynamic performance improvements relative to the B-series propeller. Numerical results indicate that changes in pitch angles exert the greatest influence on hydrodynamic efficiency, whereas variations in skew angle have the least impact. Furthermore, a comparative study examines the flow field around and downstream of the propellers under different operating conditions.

Keywords Computational fluid dynamics; Toroidal propeller; Parametric study; Blade section; Hydrodynamic coefficients

1 Introduction

Due to the extensive use of propellers in commercial and military industries, achieving high efficiency and stability under diverse operating conditions is crucial for propeller design. A comprehensive hydrodynamic analysis is necessary to optimize performance. Various propeller types, such as ducted, coaxial, and tandem propellers, have been designed and developed to suit different working requirements. This article examines the geometry and hydrodynamic performance of the toroidal propeller.

In aerospace applications, toroidal propellers are referred to as closed-loop and Boxprop types. The Boxprop propeller was the first concept aimed at reducing blade tip vortex compared with conventional propeller blades (Avellán and Lundbladh, 2013). Key features include reduced blade tip vortex, improved efficiency, lower noise levels, and enhanced structural strength. Moreover, constructive results, including noise reduction and efficiency improvements, which induce pressure reduction, are achieved by adding surfaces into conventional propellers. The geometry of a toroidal propeller is similar to tandem propellers, except that each pair of blades is joined at the tips. Furthermore, modifications to blade tip geometry considerably influence the hydrodynamic and hydroacoustic behavior of winglet propellers. The conducted studies on tandem and winglet propellers provide a solid foundational perspective on the subject. Axial displacement (distance between fore and aft propellers) and angular displacement of the aft propeller relative to the forward propeller in tandem configurations, along with the diameter ratio ($D_{\text{fore}}/D_{\text{aft}}$), have been identified as key parameters for enhancing hydrodynamic performance (Djahida and Omar, 2017; Liu and Gong, 2020). Numerical investigations of conventional propellers operating in single and tandem modes under cavitation and noncavitation conditions have demonstrated that tandem

Article Highlights

- Effect of seven geometrical parameters on the hydrodynamic performance of toroidal propellers is investigated.
- Open-water tests are numerically simulated by application of CFD techniques.
- Operational graphs of the developed toroidal propeller have been compared to a similar B-series propeller.
- The Flow characteristics behind the propellers has been analyzed.

✉ Alireza Nadery
Alireza.nadery33@gmail.com

[1] Department of Maritime Engineering, Amirkabir University of Technology, Tehran 15875-4413, Iran

[2] Department of Mechanical Engineering, Imam Hossein University, Tehran 1698715861, Iran

[3] International School of Ocean Science and Engineering, Harbin Institute of Technology, Weihai 150001, China

propellers perform better under heavy load conditions (Djahida and Omar, 2019). Simulations of the aerodynamic performance of a newly designed tandem propeller featuring an optimized profile arrangement and improved connections have shown a reduction in aerodynamic wake and an increase in aerodynamic load. Moreover, blade force distribution remains uniform along the radius, with no flow loss from one blade to another, making this configuration optimal for propellers operating at low Reynolds numbers (Kulyk et al., 2020). The efficiency of tandem propellers is higher in most operating conditions than conventional propellers with a larger expanded area ratio and additional blades. Moreover, tandem propellers offer advantages in addressing issues related to cavitation, vibration, and noise (Yao et al., 2021).

One approach to reducing cavitation and enhancing the efficiency of conventional propellers is deflecting the tips of the propeller blades. The primary benefit of a deflected blade tip is its positive impact on reducing tip vortex, a characteristic common to winglet and toroidal propellers. Numerical studies on the hydrodynamic performance of winglet propellers, conducted using Reynolds-averaged and potential theory methods, have demonstrated that winglet propellers can improve efficiency and reduce cavitation (Bertetta et al., 2012). Findings also suggest that increasing the blade curvature reduces the thrust coefficient while enhancing the efficiency of winglet propellers (Sánchez-Caja et al., 2012). A geometry optimization was implemented to improve the efficiency and diminish the cavitation performance of the winglet propellers. Geometries were simulated using the boundary element method, and the final geometry was validated using experimental approaches. The results showed that the boundary element method can be used to accurately predict the hydrodynamic performance and cavitation of winglet propellers (Gaggero et al., 2016a). Moreover, appropriate tip design has been shown to effectively reduce tip vortex formation in winglet propellers (Gaggero et al., 2016b). A similar analysis using large eddy simulation (LES) confirms the advantages of winglet propellers in mitigating cavitation and tip vortex issues (Zhu and Gao, 2019). The tip vortex and back plate cavitation (low-pressure area) can be reduced using winglet propellers, where the tip is bent toward the high-pressure region of the propeller, an innovative concept known as the endplate propeller (ENDP). Even at small expanded area ratios, the ENDP propeller can delay thrust collapse compared with conventional designs while maintaining better efficiency at low cavitation numbers (Kehr et al., 2019). Numerical investigations further reveal that while blade tip bending has minimal effect on propeller efficiency, it remarkably improves vortex cavitation at the tip. Moreover, an increase in rake angle exacerbates cavitation in winglet propellers (Gao et al., 2019).

Thus far, most studies on toroidal propellers have been conducted in the field of aerospace engineering. Research has focused on developing the initial concept of Boxprops, including the creation of an optimization platform based on a genetic algorithm for high-speed Boxprop propellers (Patrao et al., 2016). A wake analysis method enabling flow energy decomposition was also introduced (Capitao Patrao et al., 2018a). Studies on the aerodynamic and aeroacoustic performance of high-speed propellers have proven that the Boxprop generates more noise than a conventional 12-blade propeller but less than a six-blade propeller. In the initial design of the Boxprop, strong interaction between the two halves of the blades led to reduced efficiency compared with conventional propellers (Capitao Patrao et al., 2018b). Investigations indicate that the optimized front blade should bend through the downstream flow, whereas the rear blade should bend through the upstream flow, considerably reducing blade interaction (Patrao et al., 2019). Findings suggest that the angle of attack is a crucial factor influencing noise generation in Boxprops (Huang et al., 2020).

Recently, several studies on the hydrodynamic performance and geometry of toroidal propellers have been conducted. The geometry of toroidal propellers is defined by a set of specialized features, along with the common parameters used for conventional designs (Ye et al., 2023). In one numerical study, a toroidal propeller was integrated into the pump-jet propulsion system of a high-speed AUV, yielding increased hydrodynamic efficiency and achieving a speed exceeding 60 kn (Xiang and Wang, 2024). Another study evaluated the hydrodynamic performance of toroidal propellers using CFD, examining the influence of front and rear blades on tip vortex dynamics. Results indicated that increasing the advance coefficient delays tip vortex separation (Tang et al., 2024). In addition, four geometric parameters were assessed for their effects on pressure distribution at radial sections, hydrodynamic coefficients, and open-water efficiency (Wang et al., 2024). An experimental and numerical approach also investigated the influence of inclination angle, pitch, and blade count on toroidal propeller performance (Wu et al., 2024). Furthermore, the DES method was applied to investigate hydrodynamic loads and flow fields (Xu et al., 2024).

In the present study, a basic toroidal propeller geometry is developed for marine applications using numerical simulations. The effect of each geometric parameter on hydrodynamic performance is examined separately to elucidate its influence on the hydrodynamic characteristics. In addition, multiple modifications have been applied to achieve an optimal geometry. This approach is validated by comparing numerical solutions with experimental results for B-series propellers and conducting CFD simulations for the parametric study of toroidal propellers. While most similar studies have focused on a limited number of geometric parameters, the present study examines seven parameters in a comparative manner, highlighting their effects on

performance and efficiency improvements. Furthermore, the flow characteristics behind the propellers are analyzed in detail to evaluate velocity and vortex formation.

2 Numerical simulation

2.1 Governing equations

The governing equations of the fluid flow encompass the conservation of mass and Navier–Stokes equations. The Reynolds-Averaged Navier–Stokes (RANS) method is used to solve these equations, where the variables of the turbulence flow, including pressure and velocity, can be considered the sum of fluctuating and time-averaged quantities. The following equations include the averaged continuity and momentum equations for incompressible flows in Cartesian coordinates (Ferziger and Peric, 2002):

$$\frac{\partial\left(\rho\overline{u_i}\right)}{\partial x_i} = 0 \tag{1}$$

$$\frac{\partial\left(\rho\overline{u_i}\right)}{\partial t} + \frac{\partial}{\partial x_j}\left(\rho\overline{u}_i\overline{u}_j + \rho\overline{u_i'u_j'}\right) = -\frac{\partial\bar{p}}{\partial x_i} + \frac{\partial\overline{\tau}_{ij}}{\partial x_j} \tag{2}$$

where ($-\overline{\rho u_i' u_j'}$) indicates the Reynolds stress expression. An appropriate turbulence model has to be selected to solve the governing equation. The realizable k–ε two-layer turbulence model is used to solve the Reynolds stress expression (Shih et al., 1995).

The hydrodynamic performance of marine propellers can be evaluated by specifying the thrust coefficient K_T, torque coefficient K_Q, and efficiency η. If the propeller with a diameter D operates in a fluid flow with an axial velocity V and a constant angular velocity n, then it generates the thrust force T using torque Q. The main nondimensional coefficients of the propeller (open-water characteristics) may be expressed as follows (Carlton, 2007):

$$J = \frac{V}{nD} \tag{3}$$

$$K_T = \frac{T}{\rho n^2 D^4} \tag{4}$$

$$K_Q = \frac{Q}{\rho n^2 D^5} \tag{5}$$

$$\eta = \frac{J}{2\pi}\frac{K_T}{K_Q} \tag{6}$$

where J denotes the advance coefficient, K_T and K_Q represent thrust and torque coefficients, respectively, and η indicates the efficiency.

2.2 Toroidal propeller geometry

The main geometric parameters of the toroidal propeller include the radius, pitch angle, skew angle, roll angle, and alpha angle of each blade section. Rake and skew affect the distance between two coupled blades. Changing the rake and skew angles adjusts the distance between each of the two tip-joined blades along the shaft axis and the axis perpendicular to the shaft, respectively. The toroidal propeller model is presented in the front and side views in Figure 1. Additional parameters to the main geometric parameters are necessary for accurate modeling of the propeller, given the geometric complexity of the toroidal propeller. Some geometrical parameters used only in toroidal propellers are as follows:

- Roll angle: the angle of rotation of a section around the chord line. As shown in Figure 2, the roll angle reaches 90° due to the curvature of the propeller blade tip. Then, it is reversed, with the roll angle for the back propeller blade between 90° and 180°. Moreover, the roll angle at the two roots of the propeller blade is equal to zero or 180° (which is also zero).
- Alpha angle: As shown in Figure 3, the vertical angle alpha of the propeller section is defined as the angle of rotation of the section around the axis perpendicular to the skew angle line; it can change in different sections.
- Rake and skew: These parameters in the geometry of toroidal propellers represent the axial and lateral distances between two blades.

To model the toroidal propeller, the blades are divided into five sections in different radii, numbered from S1 to S5, as shown in Figure 2. Each of the front and rear blade

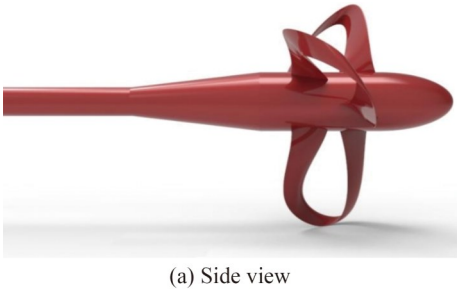

(a) Side view

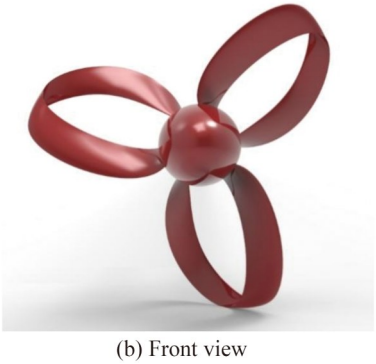

(b) Front view

Figure 1 Geometry of the toroidal propeller model

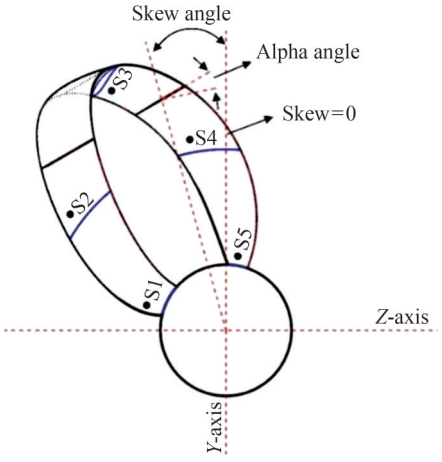

Figure 2 View of vertical angle alpha for a cross-section of a toroidal propeller blade

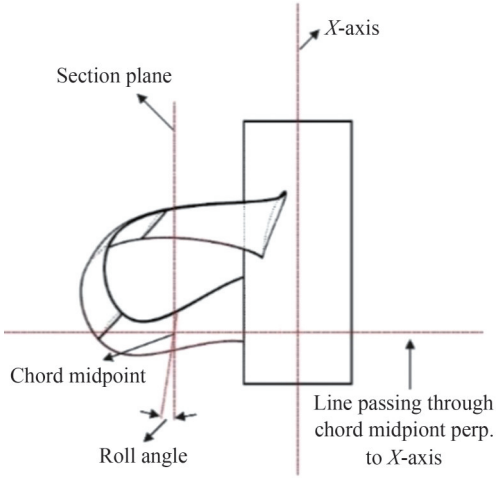

Figure 3 View of the roll angle of a toroidal propeller blade

surfaces is generated by lofting three sections. The alpha and roll angles are applied to the S3 section at the tip to specify the special geometry parameters of the toroidal propeller. Sections S1, S2, S4, and S5 follow the mathematical principles of the conventional propellers (Carlton, 2012).

The first toroidal propeller model in this study is labeled SH002, with its geometrical specifications described in Table 1 (Sharrow, 2022). Several modifications to this model are introduced in the following sections.

Table 1 Principal particulars of SH002

Principal particulars	Value
Diameter D (mm)	300
Number of blades Z	3
Hub ratio r_h/R	0.20
Pitch ratio (front blade) P_f/D	1.05
Pitch ratio (rear blade) P_r/D	1.10
Expanded area ratio EAR	0.38
Direction of rotation	Right-hand

3 Numerical results

3.1 Mesh study and validation

Experimental test results and hydrodynamic coefficient diagrams of the model are required to validate the numerical simulation. A B-series propeller is used to validate the simulation results due to the unavailability of experimental results for the toroidal propeller. A three-blade B-series propeller with an expanded area ratio of 0.3 is used for validation, and the principal particulars are presented in Table 2.

Table 2 Principal particulars of B-series propeller

Principal particulars	Value
Diameter D (mm)	240
Number of blades Z	3
Hub ratio r_h/R	0.2
Pitch ratio P/D	1.3
Expanded area ratio EAR	0.3
Direction of rotation	Right-hand

One of the widely used methods in CFD to numerically solve the RANS equations is the finite volume method (FVM). The flow field around the propeller in the computational domain is simulated using the FVM method in Star-CCM+ software. The semi-implicit method for the pressure-linked equation (SIMPLE) algorithm is used to couple the pressure and velocity (Barth and Jespersen, 1989).

Various methods can be used for the numerical simulation of submerged propellers, including moving reference frame (MRF), sliding mesh, and dynamic mesh. MRF is an appropriate topology to obtain accurate results with less calculation time, considering the large number of simulations in this parametric study (Tabib et al., 2017). In this method, where a steady solution solves the problem, two cylindrical regions are defined around the propeller. The smaller cylindrical region near the propeller forms a surface contact with the larger cylinder of the outer region. The flow around the propeller is rotated by defining the rotation in the smaller region reference frame near the propeller, the advance speed of which is specified by the inlet flow velocity definition. Other settings applied to the numerical setup are summarized in Table 3.

Table 3 Physics used in the numerical setups

Setting	Description
Time	Steady
Flow	Segregated flow
Equation of state	Constant density
Turbulence model	Realizable K-Epsilon two layer
Pressure link	SIMPLE
Wall treatment	Two layer all y^+ treatment

The numerical simulation requires defining a computational domain in three dimensions around the propeller. The computational domain used in this study is shown in

Figure 4. According to recommendations of the International Towing Tank Conference (ITTC), boundaries of the computational domain in the open-water simulation should be distant from the blades to prevent errors and disturbances in the solution. The velocity inlet and pressure outlet boundaries should be at least 2*D* and 4*D* away from the propeller surface. Moreover, the diameter of the outer cylindrical boundary should be at least 4*D*, where *D* represents the diameter of the propeller (ITTC, 2014).

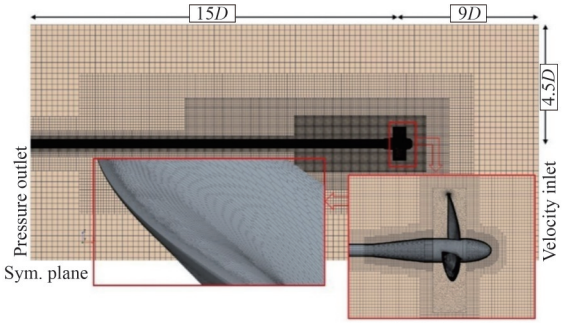

Figure 4 Surface and flow field grid of the B-series propeller simulation

Figure 4 illustrates the three conditions applied to the domain's boundaries: velocity inlet, symmetry plane, and pressure outlet. The velocity inlet boundary condition is used to define the inflow velocity into the computational domain. The pressure outlet boundary condition is applied to the flow outlet, where the boundary pressure represents the static pressure of the surrounding environment into which the fluid exits (Siemens Digital Industries Software, 2023). Lastly, the symmetry plane boundary condition is applied to the domain's side surface. This boundary can be modified without affecting the calculation results. Other types of boundaries used in other studies include velocity inlets (Sánchez-Caja et al., 2014) and slip-wall (Moghaddas et al., 2025).

The accuracy of the simulation results is highly dependent on the generated grid. When constructing an appropriate grid near the wall, the thickness of the first cell layer and the number of layers within the boundary are crucial, with both factors being strongly influenced by the selected turbulence model. In this simulation, the first boundary layer thickness and total boundary layer thickness are set to 0.000 5 and 2.557 5 mm, respectively.

The trimmed cell mesh method is used to generate a mesh in the computational domain using Star-CCM+ software. Cell sizes on the propeller surface, within the rotating area, and behind the propeller are defined with finer resolution using mesh control tools. The volume mesh inside the computational domain and the surface mesh on the propeller surface are shown in Figure 4. In addition, the value of the y^+ function on the blade and hub surfaces of the B-series propeller, set between 0 and 1 according to the k–ε turbulence model, is shown in Figure 5 (ITTC, 2014).

Another important issue regarding the grid system is the

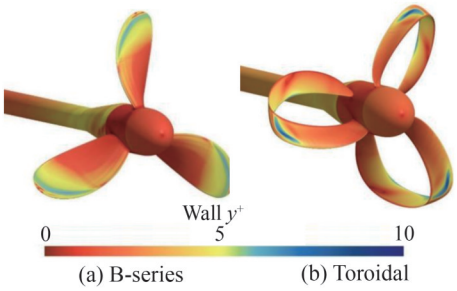

Figure 5 y^+ on the propeller surface

independence of the numerical results from the number of cells, indicating that the numerical results should be independent of the number and size of the cells. In this study, the Roache method (Roache, 1997; Celik et al., 2008) is implemented to check the grid independence. Simulation is conducted in three grid sizes: coarse, medium, and fine. In this method, s_a is expressed as follows:

$$s_a = \frac{1}{\ln r_{21}} \left| \ln \left| \frac{\varepsilon_{32}}{\varepsilon_{21}} \right| + q(s_a) \right| \tag{7}$$

and the secondary parameters shown in (7) can be expressed as follows:

$$q(s_a) = \ln \left(\frac{r_{21}^{s_a} - s}{r_{32}^{s_a} - s} \right) \tag{8}$$

$$s = 1 \cdot \operatorname{sgn} \left(\frac{\varepsilon_{32}}{\varepsilon_{21}} \right) \tag{9}$$

where r should be created for each of grids 1–3. In this equation, $r_{21} = \frac{h_2}{h_1}$, $r_{32} = \frac{h_3}{h_2}$, and h_i is the average grid size determined by the number of ith grid (N_i) and the computational domain size. The parameter ε is expressed as follows: $\varepsilon_{32} = \phi_3 - \phi_2$, $\varepsilon_{21} = \phi_2 - \phi_1$, where ϕ_i represents the solution (K_T and K_Q) of the ith grid. Other significant parameters influencing the grid convergence index (GCI) may be expressed as follows:

$$\phi_{\text{ext}}^{21} = \left(r_{21}^{s_a} \phi_1 - \phi_2 \right) \Big/ \left(r_{21}^{s_a} - 1 \right) \tag{10}$$

$$e_a^{21} = \left| \frac{\phi_1 - \phi_2}{\phi_1} \right| \tag{11}$$

$$e_{\text{ext}}^{21} = \left| \frac{\phi_{\text{ext}}^{21} - \phi_1}{\phi_{\text{ext}}^{21}} \right| \tag{12}$$

where ϕ_{ext}^{21} is the extrapolated value of the solutions; e_a^{21} and e_{ext}^{21} denote the medium and approximate relative errors, respectively. The GCI value for the medium grid is calculated using (16). The results of the grid independency study are presented in Table 4.

$$\text{GCI}_{\text{medium}}^{21} = \frac{1.25 e_a^{21}}{r_{21}^{s_a} - 1} \tag{13}$$

Table 4 Grid independency parameters for K_T and K_Q based on the Roache method in $J = 0.4$

Grid type	Number of grids		Thrust coefficient (K_T)		Torque coefficient (K_Q)	
	B-series	Toroidal	B-series	Toroidal	B-series	Toroidal
Fine	6715364	7380626	0.366800	0.415427	0.064243	0.083467
Medium	3397950	3736945	0.366304	0.416814	0.064742	0.081040
Coarse	1897514	2065470	0.365722	0.416604	0.065501	0.077179
	r_{21}		1.254924	1.254658	1.254924	1.254658
	r_{32}		1.214350	1.218519	1.214350	1.218520
	S_a		1.705306	7.522100	2.759257	2.856914
	e_a^{21}		0.001297	0.003300	0.007760	0.029077
	e_a^{32}		0.001588	0.000500	0.011725	0.047643
	$\mathrm{GCI}_{\mathrm{medium}}^{21}$		0.001297	0.000200	0.020675	0.078484

The numerical results demonstrate grid independence with a GCI value of less than one. Table 3 confirms that increasing the grid number does not substantially affect the numerical solution, thereby satisfying the grid independence criteria. Consequently, the medium grid is selected for the remaining simulations.

The B-series propeller simulation using the medium grid has been validated against existing experimental results (Van Lammeren et al., 1969). Numerical and experimental results for thrust coefficient, torque coefficient, and efficiency are presented across advance coefficients ranging from 0.2 to 1.2 with a fixed rotational speed of 70 r/s. The advance coefficient varies with the flow velocity. As shown in Figure 6, the numerical results exhibit low error values and align well with experimental data, confirming the reliability of the simulation for analyzing and developing the toroidal propeller.

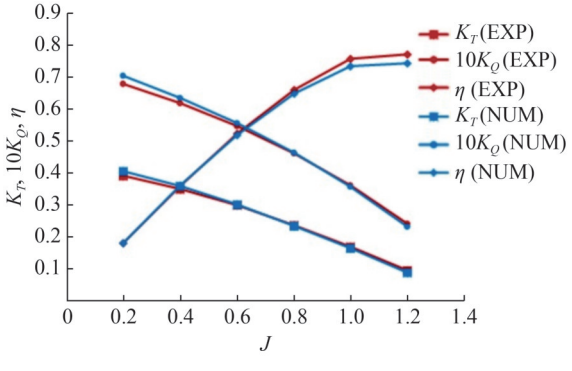

Figure 6 Comparison of hydrodynamic characteristics of the B-series propeller

3.2 parametric investigation of the toroidal propeller geometry

In this section, the effects of six parameters, namely, skew angle, pitch angle, chord length, rake, roll angle, and blade alpha vertical angle, are investigated separately. Initially, these parameters were examined separately across 12 simulations. Subsequently, seven additional conditions were simulated to evaluate the impact of multiple geometric modifications. All parametric investigations were conducted on the initial toroidal propeller geometry, SH002, which demonstrated strong performance at the initial state. During the investigation, one or more parameters were adjusted by 10% or 20%, whereas the others remained unchanged. Table 5 presents the inspected parameter variations, organized numerically. After analyzing the parameters individually, the effects of simultaneous changes to multiple parameters and the blade section on propeller performance were investigated.

4 Results and discussuion

The hydrodynamic performance diagrams for modes 1–12, in which only one parameter is modified as outlined in Table 4, are compared with the SH002 propeller in Figure 8. The first graph, shown in Figure 7(a), evaluates the effects of increased and decreased skew angles. As indicated, increasing the skew angle remarkably reduces thrust and torque coefficients, resulting in an efficiency loss relative to the SH002 propeller. Conversely, reducing the skew angle results in only a slight efficiency reduction. In the toroidal propeller geometry, the skew angle determines the angular distance between the two tip-joined blades. Different from conventional propellers, this parameter has a greater influence on hydrodynamic performance due to the heightened interaction between blade pairs.

The effect of pitch angle variation on the hydrodynamic performance of the SH002 propeller is investigated in Figure 7(b). Increasing the pitch angle delays the operating point of the propeller, whereas decreasing it negatively impacts performance. For instance, reducing the pitch angle

Table 5 Modes of investigating the effect of parameters on the toroidal propeller

Number	Propeller name	Changing parameters						
		Skew angle	Pitch angle	Chord length	Rake	Roll angle	Alpha angle	Hydrofoil
1	SH002	–	–	–	–	–	–	NACA0015
2	SH002-1	10% ↑	–	–	–	–	–	NACA0015
3	SH002-2	10% ↓	–	–	–	–	–	NACA0015
4	SH002-3	–	10% ↑	–	–	–	–	NACA0015
5	SH002-4	–	10% ↓	–	–	–	–	NACA0015
6	SH002-5	–	–	10% ↑	–	–	–	NACA0015
7	SH002-6	–	–	10% ↓	–	–	–	NACA0015
8	SH002-7	–	–	–	10% ↑	–	–	NACA0015
9	SH002-8	–	–	–	10% ↓	–	–	NACA0015
10	SH002-9	–	–	–	–	10% ↑	–	NACA0015
11	SH002-10	–	–	–	–	10% ↓	–	NACA0015
12	SH002-11	–	–	–	–	–	10% ↑	NACA0015
13	SH002-12	–	–	–	–	–	10% ↓	NACA0015
14	SH002-13	–	10% ↑	–	–	–	–	NACA2412
15	SH002-14	5% ↓	20% ↑	–	20% ↓	–	–	NACA2412
16	SH002-15	5% ↓	20% ↑	–	20% ↓	–	–	S7055
17	SH003	5% ↓	20% ↑	–	–	–	–	NACA2412
18	SH003-1	5% ↓	20% ↑	–	–	–	–	S7055
19	SH003-2	5% ↓	20% ↑	20% ↑	–	–	–	S7055

by 10% lowers the hydrodynamic efficiency of the SH002-4 propeller by 14% at an advance coefficient of 0.9. This trend is similarly observed in other advanced coefficients.

For conventional propellers, higher thrust and torque coefficients with lower efficiency are expected in the case of increasing the chord length. As the chord length in the toroidal propeller also depends on the distance between the two tip-joined blades, according to Figure 7(c), the sign of the efficiency change is similar to the mentioned case, but it is lower in magnitude, contrary to the common expectation.

The effect of the rake parameter on the hydrodynamic performance of the SH002 propeller is shown in Figure 7(d). A brief comparison between the results of changes in skew and rake parameters indicates that the axial distance between tip-joined blades, which is specified by rake angle, is a more effective parameter than the radial distance of the blades on the hydrodynamic performance of the toroidal propeller.

As shown in Figure 7(e), increasing the roll angle in SH002 decreased thrust and torque coefficients as well as efficiency. In the advance coefficient of 0.9, thrust and torque coefficients and efficiency are decreased by 12.89, 6.85, and 6.48%. Reducing the roll angle has also minimized the thrust and torque coefficients. Thus, in the advance coefficient of 0.9, the thrust coefficient and torque coefficient values are decreased by 5.18% and 5.73%, respectively, and the efficiency is increased.

Figure 7(f) illustrates that the torque coefficient is certainly sensitive to alpha angle changes. Therefore, the reverse independence of the efficiency on the alpha angle can be explained according to the amount of torque coefficient loss while the thrust coefficient is changed slightly.

Figure 9(a) shows that by increasing the pitch angle beside the changing section of the hydrofoil, the efficiency, torque coefficient, and thrust coefficient of SH002-13 increase in the advance coefficients above 0.9 compared with SH002. This increase in the advance coefficient of one is 53.55% for the thrust coefficient, 37.86% for the torque coefficient, and 11.38% for the efficiency. In Figure 8(b), SH002-3 and SH002-13 are compared to investigate the effect of the hydrofoil section on the hydrodynamic perfor-

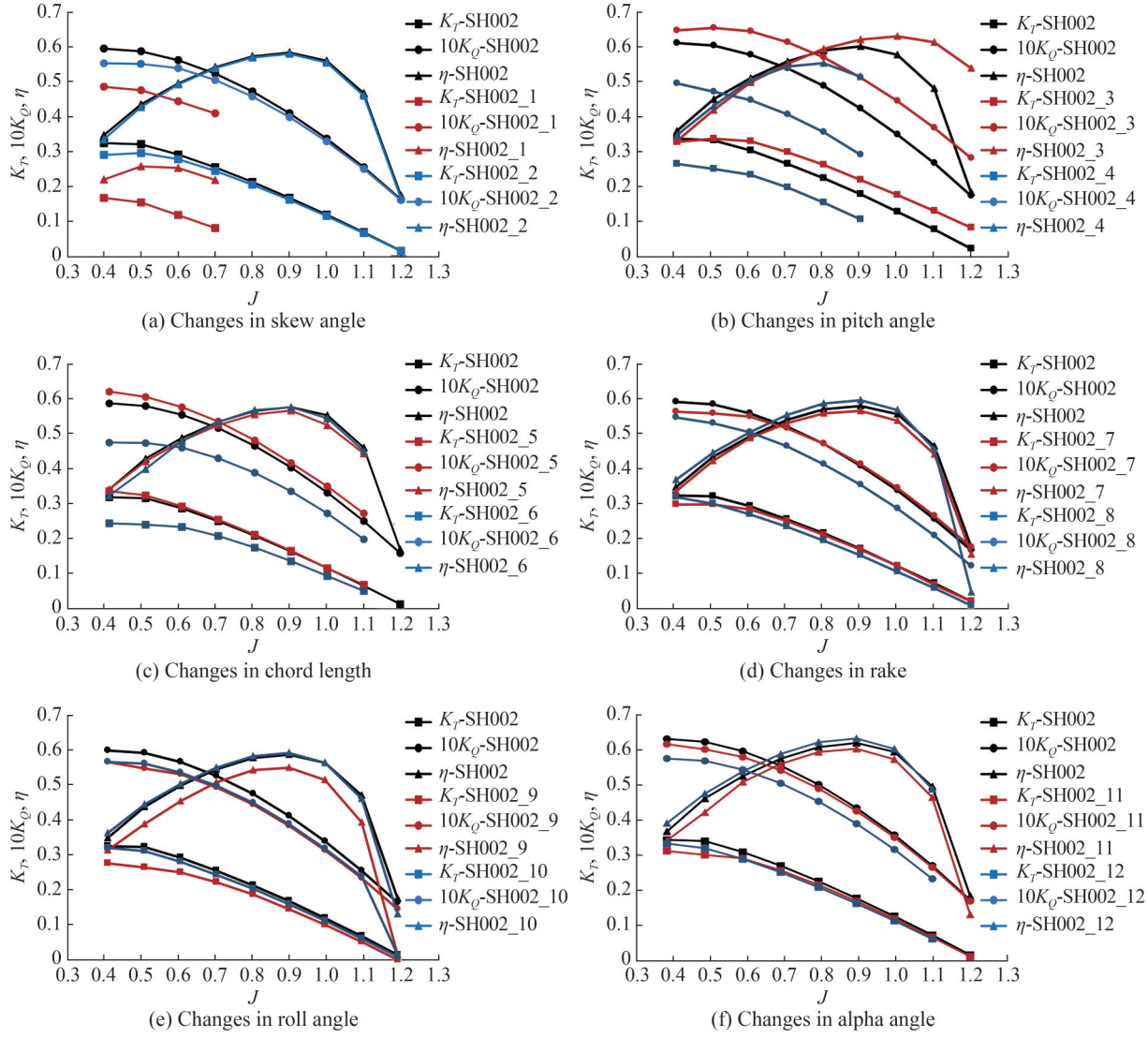

(a) Changes in skew angle (b) Changes in pitch angle

(c) Changes in chord length (d) Changes in rake

(e) Changes in roll angle (f) Changes in alpha angle

Figure 7 Hydrodynamic characteristics of the toroidal propeller under single changes in geometry parameters

mance of the propeller. In this study, three different blade sections depicted in Figure 9 are applied to the toroidal propeller to assess their effects on the hydrodynamic performance. NACA (Abbott and Von Doenhoff, 2012) and Selig (Selig et al., 1995) sections are the most examined due to their wide applications in marine and aerospace industries.

NACA2412 with 2% camber is replaced with the symmetrical section of SH002-13 in addition to the increase in pitch angle by 10%. According to the obtained results, the use of an asymmetric instead of a symmetrical section has increased the thrust coefficient, torque coefficient, and efficiency in the advance coefficients above 0.8. The variation amount in the advance coefficient of 1.1 is 14.78% for the thrust coefficient, 10.58% for the torque coefficient, and 61.9% for efficiency, representing an increase of 3.79%.

The SH002-14 and SH002-15 propellers feature a decrease in the skew angle, an increase in the pitch angle, and a reduction in the rake angle. The efficiency of SH002-14 is remarkably improved at advance coefficients greater than 0.9. In the analysis of SH002-15, shown in Figure 8(d), the skew angle, pitch angle, and rake remain the same as in SH002-14. However, a different asymmetric section with 3.3% camber (S7055) is applied to the propeller geometry. This modification increased torque and thrust coefficients at certain advance coefficients. Furthermore, the efficiency loss observed in the SH002 propeller at advance coefficients above 0.9 is recovered in SH002-15, similar to SH002-14.

To achieve a more precise analysis of the thrust force generated by the propeller, each blade of the propeller is divided into three surface components, including the front blade, rear blade, and blade tip. These parts are shown in Figure 10. The blade tip is separated from the other blades at $r = 0.75R$.

The results of the generated thrust by the surface parts of the propeller in Table 6 demonstrate that all components pro-

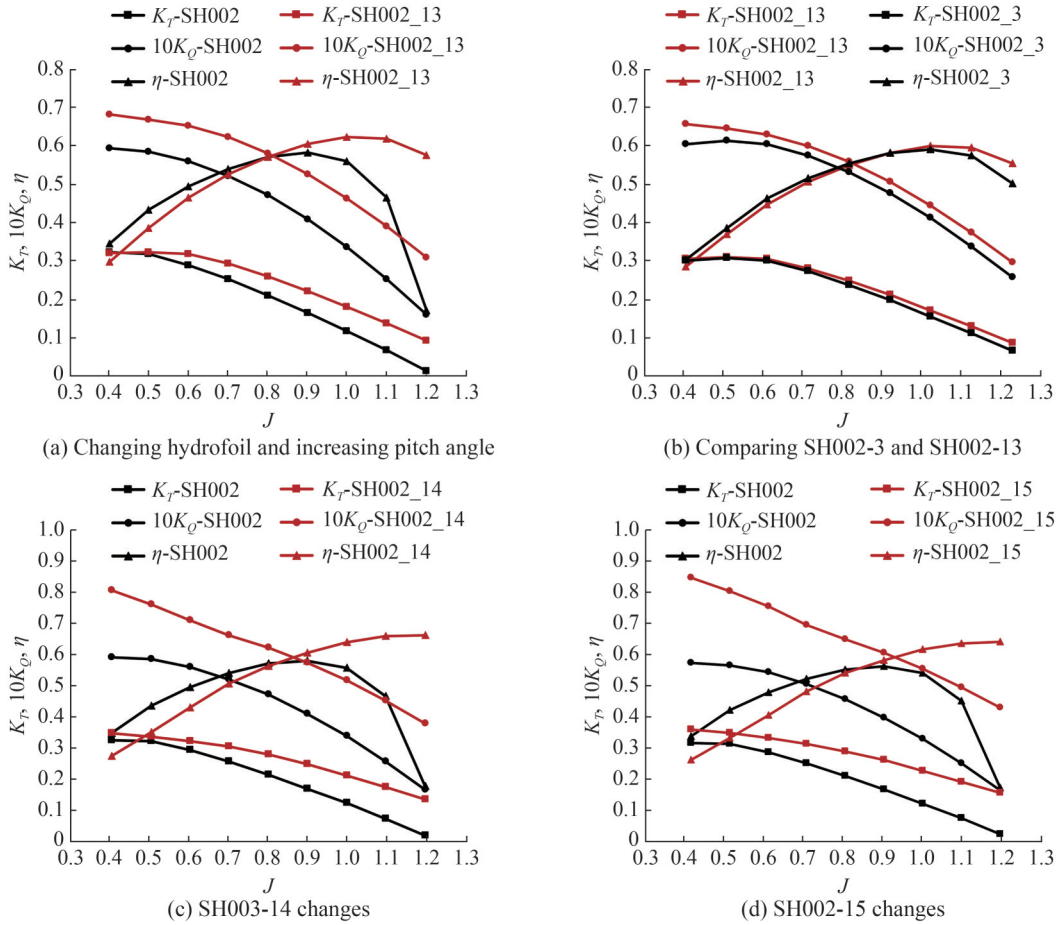

(a) Changing hydrofoil and increasing pitch angle

(b) Comparing SH002-3 and SH002-13

(c) SH003-14 changes

(d) SH002-15 changes

Figure 8 Hydrodynamic characteristics of the toroidal propeller under multiple changes in geometry parameters

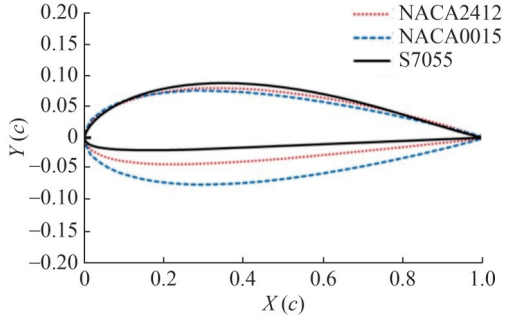

Figure 9 Blade sections used in the present study

vide positive thrust in the modified geometry. The findings indicate that the negative thrust force is produced in the rear blade, causing adverse effects on propeller performance. The undesired feature of SH002-14 propellers is resolved by increasing the pitch angle of the rear blade in SH003. Further simulations are carried out with the modified blades.

The hydrodynamic characteristics of various types of SH003 propellers are presented in Figure 11. In Figure 11(a), the hydrodynamic results of SH003 are compared with SH002-14 in the advance coefficients from 0.8 to 1.2. In approximately equal thrust coefficients, while the advance coefficient is 1.2, the efficiency has increased up to 10.8%.

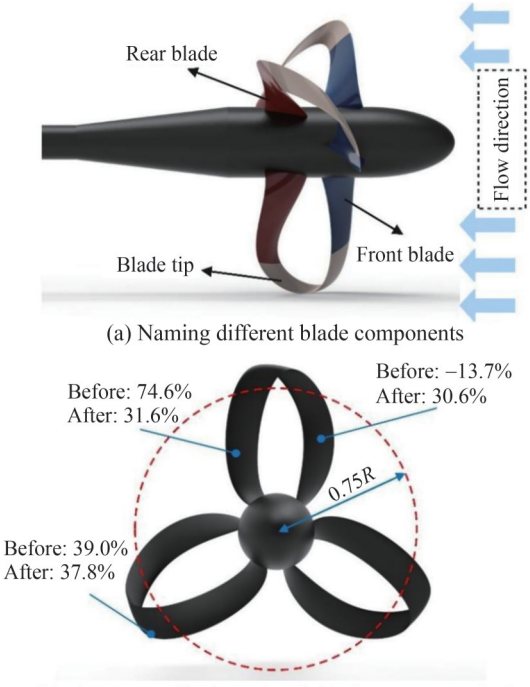

(a) Naming different blade components

(b) Thrust contribution of each blade component before and after increasing the pitch angle

Figure 10 Separated toroidal propeller blade surfaces

Table 6 Thrust force of blade surface components for SH002-14 and SH003

Blade surface part	Thrust force (N)	
	SH002-14	SH003
Front blade	579.99	257.36
Blade tip	303.53	307.67
Rear blade	−106.22	249.60
Total	777.30	814.63

The SH003 propeller is selected for comparison of the hydrodynamic performance with the B-series propeller, whose geometrical and functional characteristics are close to the developed toroidal propeller. The results of the hydrodynamic performance of the B-series propeller and the comparison of the performance of the SH003 propeller shown in the diagram of Figure 11(b) suggest that the efficiencies of the SH003 propeller and the B-series propeller are similar, whereas the thrust and torque coefficients of SH003 is lower than the B-series propeller. The results indicate that the toroidal propeller can be used in functional conditions where high efficiency and low torque are required. However, in situations where the goal is to achieve a higher thrust force, the B-series propeller can be a favorable option.

Previous results have shown that using the S7055 section in SH002-14 generates more thrust than NACA2412; changing the hydrofoil of SH003 can be an excellent modification to increase the value of the thrust load. Figure 11(c)

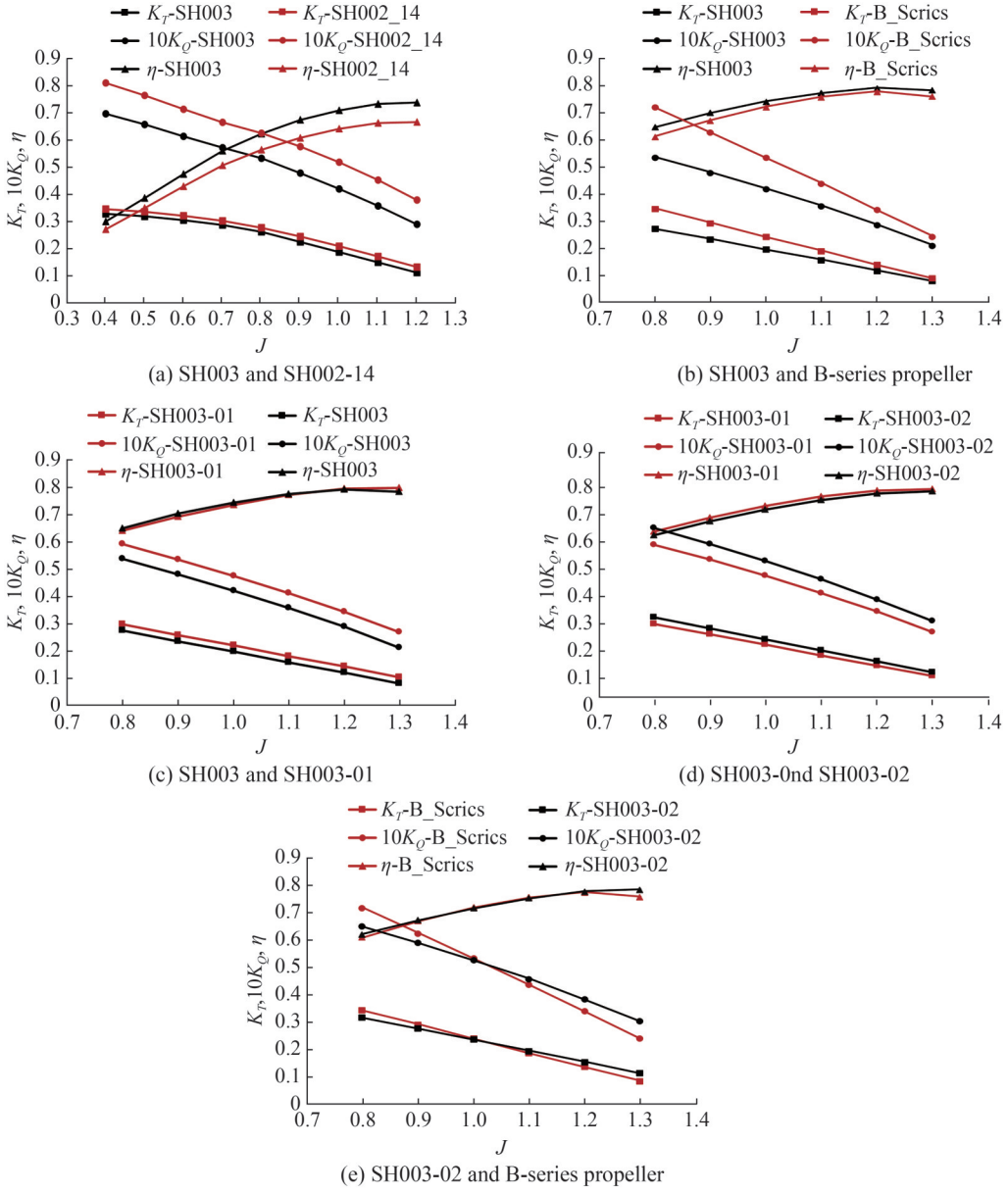

Figure 11 Hydrodynamic characteristics of various types of SH003 propellers

shows the hydrodynamic performance of the SH003 propeller with NACA2412 and the SH003-01 propeller with S7055 section. In the advance coefficient of 1.2, the torque coefficient has increased by 19.16% and the thrust coefficient by 19.33%. Previously, one of the parameters affecting propeller hydrodynamic characteristics is chord length. To improve the thrust factor of the SH003-01 propeller, the chord length of this propeller is increased by 20%, and its hydrodynamic performance is compared with the SH003-01 propeller. The new propeller is referred to as SH003-02, and the results are shown in Figure 11(d). The results illustrate that increasing the chord length results in higher thrust and torque coefficients. At an advance coefficient of 1.2, thrust and torque coefficients increase by 11.32% and 13.08%, respectively.

In accordance with the results of SH003-02, which had a better trust factor than the SH003 and SH003-01 propellers, a comparison has been made between this propeller and a B-series propeller with equal diameter. A three-blade B-series propeller with an expanded area ratio of 0.65 and a pitch ratio of 1.4 was selected for comparison. As shown in Table 7, the thrust, torque, and efficiency of the B-series propeller were evaluated using experimental data (Van Lammeren et al., 1969) to ensure the numerical simulation has sufficient accuracy.

The value of the thrust coefficient of SH003-02 is increased by 13.05% and 30.36% compared with the B-series propeller in the advance coefficient of 1.2 and 1.3, respectively. The torque coefficient is increased by 12.7% and 25.8% in the same advance coefficients.

As shown in Figure 11(e), the SH003-02 propeller has a better performance than the B-series propeller in terms of efficiency. The SH003-02 propeller has achieved an efficiency of 78.03% and 78.82% in the advance coefficients of 1.2 and 1.3, respectively. The efficiency values for SH003-02 are 0.28% and 3.6% more than the B-series propeller in advance coefficients of 1.2 and 1.3, respectively.

The difference between models with a focus on maximum efficiency and their relative advance coefficients is described in Table 8. The table demonstrates that the geometry modifications have successfully led to efficiency increases in the last models. Specifically, the maximum efficiency of the last two toroidal models is higher than that of the B-series propeller.

The axial velocity contour of the flow field around and downstream of the propellers is examined under heavy and light load conditions, as shown in Figure 12. Under heavy load conditions, the flow moves more slowly downstream of SH003-02. However, while SH003-02 nearly eliminates tip vortices in heavy load conditions, at high advance ratios, stronger tip vortices appear downstream of the toroidal propeller, an undesirable phenomenon, especially from a hydroacoustic perspective.

The cross velocity magnitude downstream of the B-series and SH002-03 at sections located at 0.5R, 1R, 2R, and 3R from the front root of the blades, as shown in Figure 13, is illustrated in Figure 14. The effect of the propeller rotation on the cross velocity value is almost eliminated at distances more than 2R. Regarding the value of the nondimensional cross velocities, this elimination is performed more successfully by SH002-03 in both conditions. In addition, the sudden increase in cross velocity around the B-series propeller has been considerably reduced in both conditions around SH003-02.

The Q-criterion function is used to identify and visualize vortices within the flow field, defining them as regions where the vorticity magnitude exceeds the rate-of-strain magnitude. Mathematically, the Q-criterion is expressed as follows:

$$Q = \frac{1}{2}\left(\| \Omega \|^2 - \| S \|^2\right) \tag{14}$$

where Ω denotes the vorticity tensor, representing the rotation rate of the fluid, and S indicates the strain rate tensor, describing the deformation rate of the fluid. To achieve a more precise analysis of vortex structures downstream of the propellers, the numerical simulation was converted from steady to unsteady physics using a time step of 5.4×10^{-5} s. This adjustment enhances vortex-capturing accuracy. Modifying the solution method from steady to unsteady leads to negligible variations in thrust and torque coefficients, with a maximum deviation of 0.4% in $J = 0.4$ for SH003-02.

Table 7 Verification of the B-series propeller used in the comparative analysis

J	K_T			K_Q			η		
	CFD	EFD	Error (%)	CFD	EFD	Error (%)	CFD	EFD	Error (%)
0.4	0.4872	0.4844	−0.5916	0.0976	0.1015	3.8365	0.3179	0.3039	−4.6047
0.6	0.3936	0.3995	1.4622	0.0808	0.0850	4.8997	0.4652	0.4490	−3.6146
0.8	0.3086	0.3086	−0.0227	0.0647	0.0671	3.6257	0.6072	0.5851	−3.7857
1.0	0.2147	0.2154	0.3170	0.0490	0.0486	−0.7742	0.6978	0.7055	1.0829
1.2	0.1259	0.1237	−1.8231	0.0322	0.0309	−4.2850	0.7473	0.7654	2.3608

Table 8 Maximum efficiency and relative advance coefficients of different geometry cases

Number	Propeller name	Changes	Max. efficiency	J at max. efficiency
1	SH002	–	58.30	0.9
2	SH002-1	Skew	25.69	0.5
3	SH002-2	Skew	57.92	0.9
4	SH002-3	Pitch	61.28	1.0
5	SH002-4	Pitch	53.59	0.8
6	SH002-5	Chord	57.30	0.9
7	SH002-6	Chord	58.28	0.9
8	SH002-7	Rake	56.78	0.9
9	SH002-8	Rake	59.90	0.9
10	SH002-9	Roll	54.52	0.9
11	SH002-10	Roll	56.75	0.9
12	SH002-11	Alpha	56.75	0.9
13	SH002-12	Alpha	59.54	0.9
14	SH002-13	Pitch–hydrofoil	62.31	1.0
15	SH002-14	Skew–pitch–rake–hydrofoil	66.60	1.2
16	SH002-15	Skew–pitch–rake–hydrofoil	66.47	1.2
17	SH003	Skew–pitch–hydrofoil	73.83	1.2
18	SH003-1	Skew–pitch–hydrofoil	79.42	1.2
19	SH003-2	Skew–pitch–chord–hydrofoil	78.58	1.2
20	B-series	–	74.53	1.2

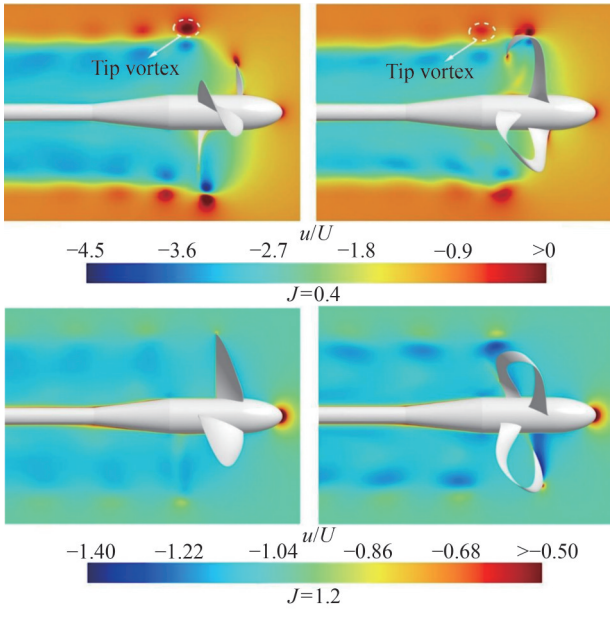

Figure 12 Axial velocity contours around and downstream the propellers, left: B-series, right: SH003-02

Figure 12 illustrates that SH003-02 has poorly formed downstream flow in the light load condition compared with the B-series propeller. Moreover, SH003-02 generates a higher vortex volume in the light load condition, as shown in Figure 15. The mean vorticity values for all cases across two different Q-criteria ranges are presented in Table 9. In

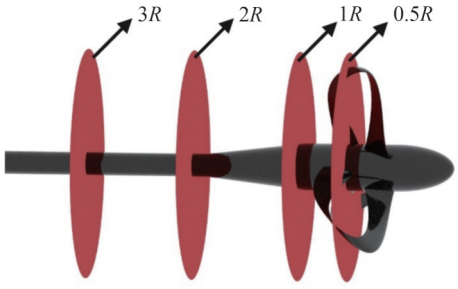

Figure 13 Sections of the cross velocity contours

higher Q-criteria ranges, where high vorticity values are more probable, the mean vorticity magnitude of the toroidal propeller is reduced by 7.5% and 18.21% in heavy and light load conditions, respectively. This improvement in hydrodynamic performance can subsequently improve the hydroacoustic behavior of the propeller, especially in heavy load conditions.

Pressure coefficients contour on the surfaces of toroidal and B-series propellers are presented in Figure 16. It is obtained using the following equation:

$$C_P = \frac{P - P_0}{\frac{1}{2}\rho U_R^2} \tag{15}$$

where U_R is defined as the magnitude of the resultant rota-

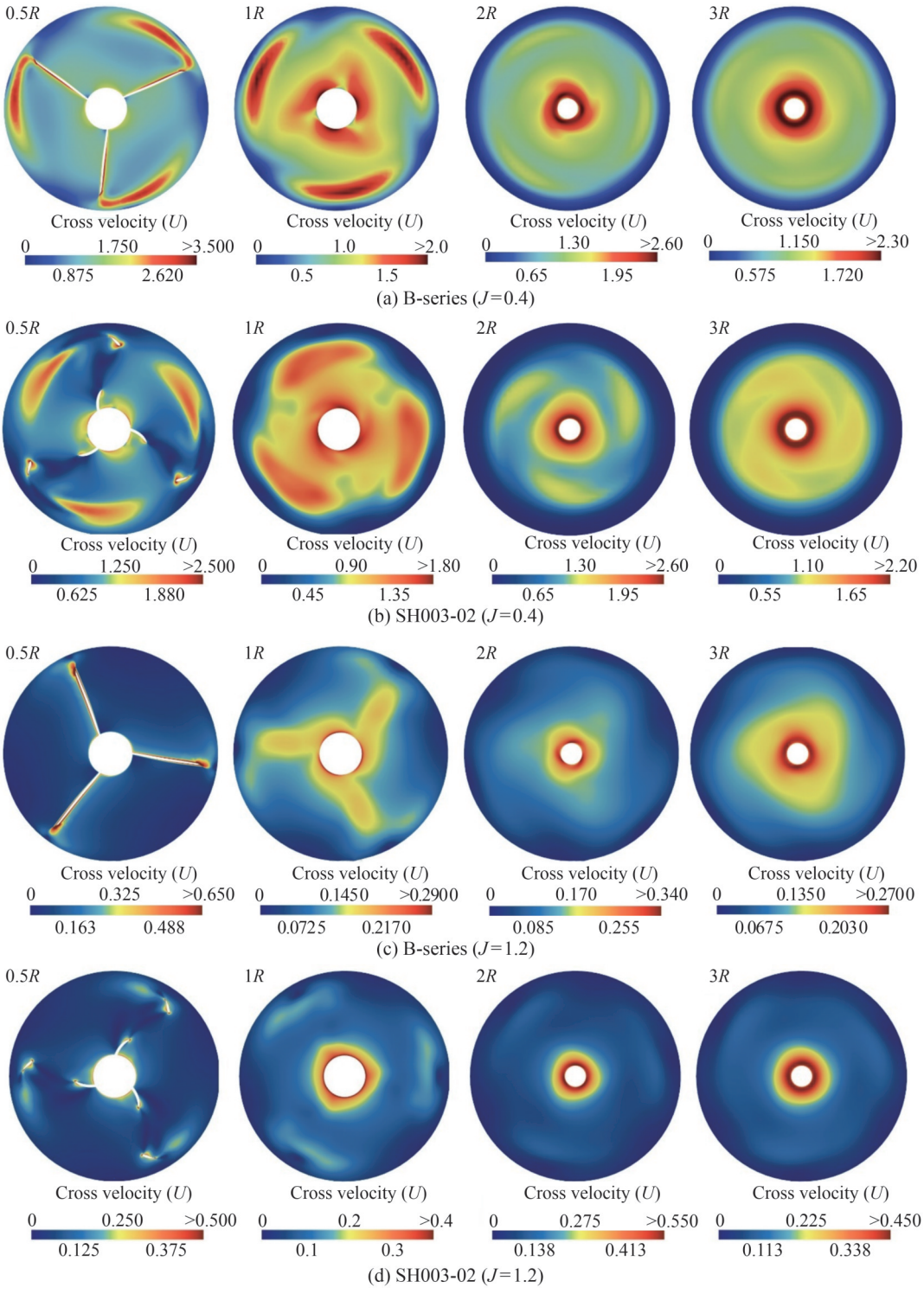

Figure 14 Nondimentional axial velocity contours downstream of the propellers in different load conditions

tional and axial velocities of the inflow to the propeller: ($U_R = \sqrt{V_A^2 + (2\pi rn)^2}$), and P_0 is the reference pressure, given by the sum of atmosphere pressure and hydrostatic pressure. For the front and rear blades of the toroidal propeller, the pressure on the suction side is considerably lower than on the pressure side. A pressure drop is also observed at the tip of the toroidal propeller, which can be rationalized by considering the roll angle. The pressure coefficient at the front and back sides of the B-series propeller blade surfaces has a smoother distribution than the toroidal propeller due to the absence of additional surfaces near the blades. Phase transition and migration are key factors in

cavitation analysis, particularly when the operational depth is insufficient (Preso et al., 2024; Zhang et al., 2024). Given the unique shape of the toroidal propeller, preventing cavitation on the suction side of the rear and front blades, as well as at the blade tip, must be fully considered.

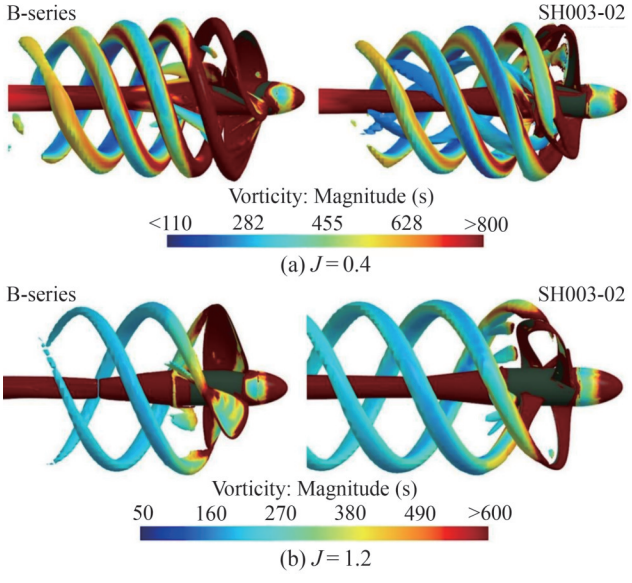

Figure 15 Vorticity magnitude in the vortex volume of B-series and toroidal propeller with Q-criteria -10^6 s^{-2} at different advance ratios

Table 9 Value of mean vortex volume in different conditions

Propeller type	Q-criteria range ($1/s^2$)	Mean vorticity magnitude (1/s)			
		$J = 0.4$	Improvement (%)	$J = 1.2$	Improvement (%)
B-series	(0, 1 000 000)	67.7		194.3	
	(500, 1 000 000)	755.5		435.4	
Toroidal	(0, 1 000 000)	78.3	−15.65	171.3	+11.83
	(500, 1 000 000)	698.8	+7.50	356.1	+18.21

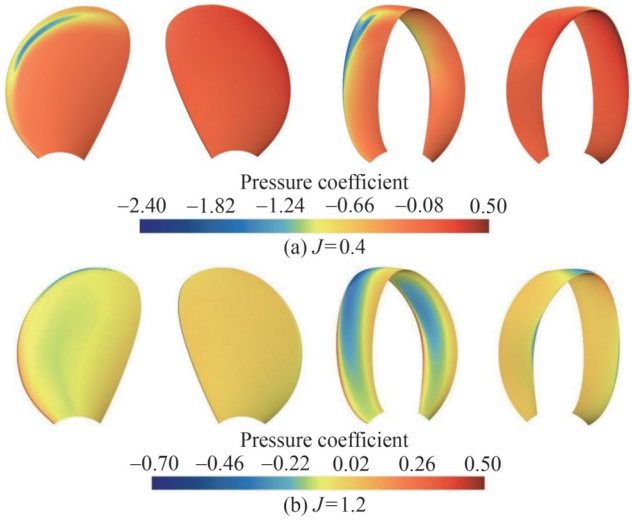

Figure 16 Pressure coefficient contour propeller blade surfaces at two working conditions

5 Conclusions

This study introduces the geometrical parameters of the toroidal propeller and examines their effects under various operating conditions. The findings provide a valuable framework for designing new toroidal propellers. The thrust, torque, and efficiency of different toroidal propeller geometries have been numerically analyzed. Due to the absence of precise experimental tests, the validated simulation results of the B-series propeller serve as a reliable reference for assessing hydrodynamic performance. Modifying the propeller's parameters can have positive and negative impacts on performance. The following results summarize the impact of these geometrical changes:

1) According to conducted studies, the following parameters have the greatest effect on hydrodynamic efficiency, in order: pitch angle, roll angle, alpha angle, rake, section's chord length, and skew angle.

2) The pitch angle is identified as the most influential geometric parameter in enhancing the hydrodynamic performance of the toroidal propeller, increasing open-water efficiency to a maximum of 79.42% and it is the main factor for preveting negative thrust of the blades.

3) Changing the blade sections remarkably affects the hydrodynamic performance of the propeller. The numerical results indicate that the S7055 hydrofoil is the most suitable among NACA0015, NACA2412, and S7055.

4) Regarding the flow field analysis behind the propellers, this toroidal propeller works more appropriately under heavy load conditions.

5) According to the vorticity analysis, this toroidal propeller has not performed as well as the B-series propeller in the light load condition. However, in higher Q-criteria ranges, the analysis shows that the toroidal propeller reduces mean vorticity by 7.5% and 18.21% in heavy and light load conditions, respectively.

6) Increased curvature complexity in the toroidal propeller's blade surfaces results in stronger pressure distribution across the blades than the B-series propeller. Therefore, greater attention should be provided to minimizing the risk of cavitation.

Due to lack of precise experimental data of toroidal propellers, conducting experimental tests can significantly enhance the strength of the future works. Another field of study that can be beneficial for developing this kind of propeller is investigation of the noise and cavitation phenomena. Furthermore, further investigations need to be conducted to reduce vortex formation in the toroidal propeller under light load conditions. Lastly, Analysis of hydrodynamic performance under nonuniform and unsteady conditions is considered an interesting field to be studied.

Acknowledgement We would like to extend our sincere appreciation to the High Performance Computing Research Center (HPCRC) at Amirkabir University of Technology for its invaluable resources and

facilities that were essential to the success of this study.

Competing interest Hassan Ghassemi is an editorial board member for the Journal of Marine Science and Application and was not involved in the editorial review, or the decision to publish this article. All authors declare that there are no other competing interests.

References

Abbott IH, Von Doenhoff AE (2012) Theory of wing sections: including a summary of airfoil data. Courier Corporation

Avellán R, Lundbladh A (2013) Boxprop, a forward-swept joined-blade propeller. ISABE-2013-1108

Barth T, Jespersen D (1989) The design and application of upwind schemes on unstructured meshes. 27th Aerospace Sciences Meeting, Reno, USA, 366

Bertetta D, Brizzolara S, Canepa E, Gaggero S, Viviani M (2012) EFD and CFD characterization of a CLT propeller. International Journal of Rotating Machinery 2012: 348939. https://doi.org/10.1155/2012/348939

Capitao Patrao A, Grönstedt T, Avellán R, Lundbladh A (2018a) Wake energy analysis method applied to the Boxprop propeller concept. Aerospace Science and Technology 79: 689-700. https://doi.org/10.1016/j.ast.2018.06.018

Capitao Patrao A, Lindblad D, Lundbladh A, Grönstedt T (2018b) Aerodynamic and aeroacoustic comparison of optimized high-speed propeller blades. 2018 Joint Propulsion Conference, 1-16. https://doi.org/10.2514/6.2018-4658

Carlton J (2007) Marine propeller and propulsion. 2nd Edition. Oxford, Bodmin Cornwall, 89-92

Carlton JS (2012) Marine propellers and propulsion. 3rd edition. Butterworth-Heinemann, Vol. 163. https://doi.org/10.1680/maen.2010.163.4.182

Celik IB, Ghia U, Roache PJ, Freitas CJ, Coleman H, Raad PE (2008) Procedure for estimation and reporting of uncertainty due to discretization in CFD applications. Journal of Fluids Engineering 130(7): 0780011-0780014. https://doi.org/10.1115/1.2960953

Djahida B, Omar I (2017) Impact of some geometrical aspects on the tandem co-rotating propeller hydrodynamic characteristics. Brodogradnja: Teorija i Praksa Brodogradnje i Pomorske Tehnike 68(1): 107-123

Djahida B, Omar I (2019) Numerical simulation of the cavitating flow around marine co-rotating tandem propellers. Brodogradnja 70(1): 43-57. https://doi.org/10.21278/brod70104

Ferziger JH, Peric M (2002) Computational methods for fluid dynamics. Third edition. Springer, Berlin

Gaggero S, Gonzalez-Adalid J, Perez Sobrino M (2016a) Design of contracted and tip loaded propellers by using boundary element methods and optimization algorithms. Applied Ocean Research 55: 102-129. https://doi.org/10.1016/j.apor.2015.12.004

Gaggero S, Gonzalez-Adalid J, Sobrino MP (2016b) Design and analysis of a new generation of CLT propellers. Applied Ocean Research 59: 424-450. https://doi.org/10.1016/j.apor.2016.06.014

Gao Hongtao, Zhu Wencai, Liu Yutong, Yan Yuying (2019) Effect of various winglets on the performance of marine propeller. 86 (January): 246-256. https://doi.org/10.1016/j.apor.2019.03.006

Huang Z, Yao H, Sjögren O, Lundbladh A, Davidson L (2020) Aeroacoustic analysis of aerodynamically optimized joined-blade propeller for future electric aircraft at cruise and take-off. Aerospace Science and Technology 107: 106336

ITTC (2014) Practical guidelines for ship self-propulsion CFD. ITTC-Recommended Procedures and Guidelines, 9

Kehr Y, Xu H, Kao J (2019) On the development and verification of diffused endplate propeller. Sixth International Symposium on Marine Propulsors SMP'19, Rome, Italy

Kulyk M, Kirchu F, Hanesh H (2020) A numerical study of performance of the small-size uav pushing tandem propeller with joined blades. Eastern-European Journal of Enterprise Technologies 2(7(104)): 40-48. https://doi.org/10.15587/1729-4061.2020.199486

Liu Y, Gong Q (2020) Numerical investigation on the flow characteristics and hydrodynamic performance of tandem propeller. Applied Ocean Research 101(July): 102292. https://doi.org/10.1016/j.apor.2020.102292

Moghaddas A, Gholipor M, Nadery A, Bahrami H (2025) Investigating the effect of blade tip bending (winglet) on efficiency and occurrence of cavitation of a submerged propeller. Ocean Engineering 319: 120254

Patrao AC, Grönstedt T, Lundbladh A, Villar GM (2019) Wake analysis of an aerodynamically optimized boxprop high-speed propeller. Journal of Turbomachinery 141(9): 1-48. https://doi.org/10.1115/1.4043974

Patrao AC, Montero Villar G, Takachi Tomita J, Bringhenti C, Avellan R, Lundbladh A, Grönstedt T (2016) An optimization platform for high speed propellers. Aerospace Technology Congress, Solna, Stockholm, 1-17

Preso DB, Fuster D, Sieber AB, Obreschkow D, Farhat M (2024) Vapor compression and energy dissipation in a collapsing laser-induced bubble. Physics of Fluids 36(3): 033342

Roache PJ (1997) Quantification of uncertainty in computational fluid dynamics. Annual Review of Fluid Mechanics 29(1): 123-160

Sánchez-Caja A, González-Adalid J, Perez-Sobrino M, Saisto I (2012) Study of end-plate shape variations for tip loaded propellers using a RANSE solver. 29th Symposium on Naval Hydrodynamics, Gothenburg, Sweden

Sánchez-Caja A, González-Adalid J, Pérez-Sobrino M, Sipilä T (2014) Scale effects on tip loaded propeller performance using a RANSE solver. Ocean Engineering 88: 607-617

Selig MS, Lyon CA, Giguere P, Ninham CP, Guglielmo JJ (1995) Summary of low-speed airfoil data: Volume 1. SoarTech Publications

Sharrow GC (2022) Propeller. US20220135195A1. United States Patent Office

Shih TH, Liou WW, Shabbir A, Yang Z, Zhu J (1995) A new $k-\varepsilon$ eddy viscosity model for high reynolds number turbulent flows. Computers & Fluids 24(3): 227-238

Siemens Digital Industries Software (2023) STAR-CCM+ [Version 2402.0001] Tutorial Guide. Siemens Digital Industries Software, Munich, Germany

Tabib M, Siddiqui MS, Rasheed A, Kvamsdal T (2017) Industrial scale turbine and associated wake development-comparison of RANS based Actuator Line Vs Sliding Mesh Interface Vs Multiple Reference Frame method. Energy Procedia 137: 487-496

Tang Z, He W, Li Z (2024) Research on the open-water performance and tip-vortex of toroidal propeller. 34th International Ocean and Polar Engineering Conference, Rhodes, Greece, ISOPE-I-24-582

Van Lammeren WPA, Van Manen JD, Oosterveld MWC (1969) The Wageningen B-screw series. The Society of Naval Architects and Marine Engineers, New York, USA

Wang C, Liu S, Xia K, Wang C, Ye L (2024) Numerical research on hydrodynamic performance of toroidal propeller under the influence of geometric parameters. Ocean Engineering 314: 119704

Wu J, Wang Q, Deasy H, Hang J (2024) A study on the effect of

toroidal propeller parameters on efficiency and thrust. Energies 17(23): 5938

Xiang Y, Wang W (2024) Hydrodynamic performance evaluation of pump-jet propulsion based on the toroidal propeller. Ocean Engineering 311(P2): 118932. https://doi.org/10.1016/j.oceaneng.2024.118932

Xu P, Guo Y, Ye L, Song K (2024) Hydrodynamic performance of toroidal propeller based on detached eddy simulation method. Journal of Marine Science and Engineering 12(12): 2132

Yao H, Liu Y, Zhang H, Zhang Q (2021) Comparative study on hydrodynamic performance and induced pressure of new canard tandem propellers and conventional propellers. Ocean Engineering 221: 108566. https://doi.org/10.1016/j.oceaneng.2021.108566

Ye Liyu, Wang Chao, Sun Cong, Guo Chunyu (2023) Mathematical expression method for geometric shape of toroidal propeller. Chinese Journal of Ship Research 19(3): 224-233

Zhang AM, Li SM, Xu RZ, Pei SC, Li S, Liu YL (2024) A theoretical model for compressible bubble dynamics considering phase transition and migration. Journal of Fluid Mechanics 999: A58

Zhu W, Gao H (2019) A numerical investigation of awinglet-propeller using an LES model. Journal of Marine Science and Engineering 7(10): 333. https://doi.org/10.3390/jmse7100333